JOURNAL OF APPLIED ELECTROCHEMISTRY **27** (1997) 928–938

Mathematical modelling of aluminium cells with prebaked anodes Part II: Current distribution and influence of sideledge

J. ZORIC, I. ROUŠAR[†]

Institute of Chemical Technology, Department of Inorganic Technology, 166 28 Prague 6, Czech Republic

J. THONSTAD[*]

Norwegian Institute of Technology, Department of Electrochemistry, N-7034, Trondheim, Norway

T. HAARBERG

Hydro Aluminium a.s., Teknologisenter, PO Box 303, N-5870 Ovre Ardal, Norway

Received 20 August 1996; revised 6 December 1996

The current distribution at the electrodes in an industrial aluminium cell with prebaked anodes was calculated. The difference between the primary and secondary current distribution was determined for three different gaps between anodes or between anode and sidewall (2.5, 10 and 30 cm). The calculated current densities at the vertical sides of the anode were higher for the secondary current distribution than for the primary (almost double at the uppermost part of the anode), while the differences were much smaller at the cathode (6–20%). If the conducting carbon sidelining is exposed to the electrolyte it will draw an average current density of 0.045 A cm^{-2} for a 30 cm distance to the cathode. If all this current leads to the formation of aluminium carbide with subsequent dissolution into the electrolyte, the sidelining will corrode at a rate of 0.08 cm d^{-1} of exposure. The influence of the shape and position of the ledge on the anode current distribution was studied. When the distance between the ledge and anode was greater than 15 cm the shape of the sideledge does not affect the anode current densities significantly, while the current density at the upper part of the anode increases with increasing distance.

List of symbols

a, b Tafel coefficients for the anodic overvoltage (V) and (V $decade^{-1}$), respectively (see Equation 1)
E electrode potential (V)
I current (A)
j current density (A cm^{-2})
$\bar{j}$ averaged current density for the electrode (A cm^{-2})
x, y, z distances in the x, y or z directions, respectively (cm)
Wa_A, Wa_C Wagner numbers (see Equations 12 and 13)
L characteristic length (see Equations 14–16)

Greek symbols
φ Galvani potential (V)
ρ specific resistivity (Ω cm)
γ angle between the sideledge and the cathode (see Fig. 1.)
η overvoltage (V)

Subscripts
A anode
b bottom flat part of the anode
C cathode
E electrolyte
x value in the x direction (x component)
y value in the y direction (y component)
rev reversible
r dimensionless parameters (see Equations 14–16)

Superscript
S in the electrolyte at the electrode/electrolyte interface (see Equations 1–4)

1. Introduction

The current distribution in industrial aluminium cells has been studied extensively [1–13]. Different approaches have been made to study the current distribution, that is, primary current distribution [1, 3] and secondary current distribution (see below) [2, 4, 8, 9]. The sidewalls of aluminium cells are covered with a ledge of frozen electrolyte (cryolite), and sideledge problems have been studied [14–23] by measuring the shape of the sideledge using probing techniques and also by means of mathematical modelling.

[*] Author to whom correspondence should be addressed.
[†] Deceased

In previous work [4] we calculated the current distribution in aluminium cells with Søderberg anodes for the measured shape of the anode and also of the sideledge [7]. In Part I of the present study [9] mathematical modelling of the current distribution and the steady state shapes of anodes in industrial aluminium cells with prebaked anodes was presented. This work is a continuation of that study [4, 7, 9], giving information both about the current distribution along the electrodes and the effect of the sideledge. The following questions are of interest: (i) what are the differences in calculated current densities along the electrodes for the two approximations of current distribution: primary current distribution (PCD) and secondary current distribution (SCD), (ii) what is the influence of the sideledge on the current densities, especially: (a) the effect of the sideledge-anode distance and (b) the effect of the shape of the sideledge.

This study consists of three parts, all dealing with a solution of the Laplace equation (LE) in 2D cross sections of a prebake aluminium cell. The LE was solved by using the finite element method. The computing mesh was generated by a commercial software, and a solver for the problems mentioned below was developed by the authors. The following problems were studied:

(i) The difference between the primary current distribution (PCD), with constant overvoltage at any current density, and the secondary current distribution (SCD), with overvoltage depending on current density, was calculated using a typical cell geometry and working parameters for industrial aluminium cells. The primary current distribution is easier to calculate because the LE can be solved by many versions of standard commercial software without any need of additional software. The difference between primary and secondary current distribution may serve to illustrate whether primary current distribution can be used for a given purpose. A similar analysis can be found in the literature for other electrolysis cells (e.g., for the Hull cell [5]).

(ii) The second part addresses the effect of the presence of a ledge of frozen electrolyte on the sidewall on the current distribution and the effect of the absence of a ledge. During normal cell operation the sidelining is protected by a layer of frozen electrolyte, the so-called sideledge. But from time to time, the frozen ledge may melt away partly or completely, and the sidelining will be exposed to the molten electrolyte, acting as cathode [6]. Three cases were calculated: (a) with the sidewall completely insulated by ledge, (b) partially insulated and (c) completely conducting, respectively, giving current densities along the sidewall and the total current passing through it.

(iii) The current distribution along the electrodes was calculated for realistic ledge shapes. The shape of the sideledge, the angle between the sideledge and the horizontal (denoted as the cathode in Fig. 1), and the distance between the sideledge and the anode side were varied to see how they influence the current distribution.

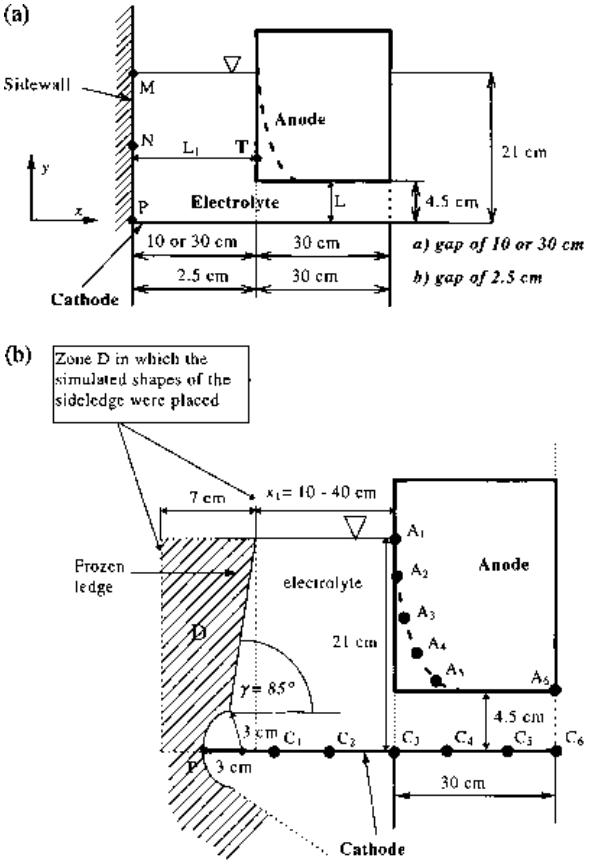

Fig. 1. (a) Vertical cross section of an aluminium electrolysis cell with prebaked anode. Width outside gap: (a) outside gap 10 or 30 cm and (b) 2.5 cm. The black zone represents the initial shape of the anode. The dashed line represents the steady state anode shape for SCD, calculated for the width of the outside gap $L_1 = 30$ cm. (b) Vertical cross section of a cell with typical ledge shape. Width outside gap defined by x_1. Black zone represents initial profile of anode. Dashed line represents steady state anode profile for SCD: width outside gap, $x_1 = 30$ cm. In zone D different shapes of the sideledge were tested. Calculated c.d. in points A_1–A_6 and C_1–C_6 are given in Table 3.

2. Theory

2.1. *Difference between primary and secondary current distribution*

The current from the sides of the anode affects the current distribution on the cathode, especially in the wide central channel and in the peripheral channel between the anodes and the sidelining. Different approximations can be used, depending on the application, for example, primary current distribution [1, 3], or secondary current distribution [2, 4, 8, 9]. For some complex analyses including several different fields (electrical, thermal, concentration) the tertiary current distribution [25] should be used, demanding very good and well balanced boundary conditions. Some of the calculations can be carried out successfully just with primary current distribution [1, 3],

while others [2, 4, 8, 9] require a high accuracy and the secondary current distribution must be used. The level of approximations for SCD can also vary from a linearization of the electrode polarization curve [8] to software solutions dealing with an empirical equation describing the dependence of the overvoltage against current density [2, 9].

In this study two different approximations of the boundary conditions were used: the PCD with constant overvoltage at any current density and the SCD with overvoltage depending on current density. A 2D cross-section of a commercial cell was considered, and the electric field in the cell was calculated under steady state conditions. The overvoltages for both anode and cathode were introduced for SCD. Two anode profiles were used for calculations: (a) the initial rectangular shape of the anode after a new anode has been set and (b) the rounded shape at steady state conditions. The steady state profile for this purpose was obtained by mathematical modelling [9]. These profiles were compared with those measured on anodes from a cell [9].

Vertical 2D cross sections represented planes located at the centres of the sides of the anode in the cell as shown in Fig. 1(a) and (b). Three different gaps to a neighbouring anode or to the sidewall [9] were considered: (i) 30 cm which represents a typical distance in the peripheral channel, (ii) 10 cm which represents half the width of a central channel, and (iii) 2.5 cm which represents half the distance to a neighbouring anode. Because of the geometrical symmetry between two anodes with identical profiles, the central boundary plane can also be considered as an insulating plane, so that the calculation carried out represents the cases when the distances between two anodes are 60, 20 and 5 cm, respectively. All the above mentioned cases were calculated using appropriate boundary conditions for PCD or for SCD.

For PCD the following boundary conditions were used. The inner potential of the electrolyte at the anode surface is given by

$$\varphi_A^S = U_{cell} - E_{rev,A} - a_A - b_A \log(\bar{j}) \qquad (1)$$

where $\bar{j}$ is the averaged current density for the electrode, chosen to be $0.75\,A\,cm^{-2}$. The selected Tafel coefficients were $a_A = 0.5\,V$ and $b_A = 0.25\,V$ decade^{-1}, and $|E_{rev,A}| = 1.23\,V$ (for more information see [9]). As can be seen from Equation 1, for PCD φ_A^S is a constant.

The inner potential of the electrolyte at the cathode surface is

$$\varphi_C^S = -E_{rev,C} - b_C \bar{j} \qquad (2)$$

and φ_C^S is a constant for PCD.

The boundary conditions for SCD were defined assuming that the electrode potential depends on the current density, as outlined in [25]. The temperature and the composition of the electrolyte were considered to be constant. In this case the following boundary conditions were used. The inner potential of the electrolyte at the anode surface is given by

$$\varphi_A^S = U_{cell} - E_{rev,A} - a_A - b_A \log(j_A) \qquad (3)$$

where a_A and b_A are the Tafel coefficients whose values are given above.

The inner potential of the electrolyte at the cathode surface is given by

$$\varphi_C^S = -E_{rev,C} - b_C j_C \qquad (4)$$

where $b_C = 0.08\,\Omega\,cm^2$ is the coefficient for the cathode [3] and

$$E_{rev,C} = 0 \qquad (5)$$

The assumptions made for the solution of the Laplace equation (LE) in the interelectrode space are outlined in Part I [9].

To simplify the presentation of the results, the border between the side and the underside of the anode was defined as shown in Fig. 2. The side of the anode extends from point A to G, while the underside begins at point G and covers the flat bottom part of the anode, the so-called working face of the anode, that is, in this case up to point K.

2.2. *Current through a sidewall which is only partly covered by ledge*

During normal cell operation the sidelining is protected by a layer of frozen electrolyte. But as mentioned above, parts of the ledge may melt away and the exposed sidelining material will be acting as cathode [6]. Calculations were carried out assuming that the carbon sidelining has the same potential as the aluminium cathode. In reality the situation is far more complex, and there may be a potential difference. Initially sodium will be discharged, dissolving into the electrolyte and into the carbon sidelining, followed by aluminium carbide (Al_4C_3) formation on the surface,

$$\frac{4}{3}AlF_4^-(liq) + C(s) + 4e^- = \frac{1}{3}Al_4C_3(s) + 4F^-(liq) \qquad (6)$$

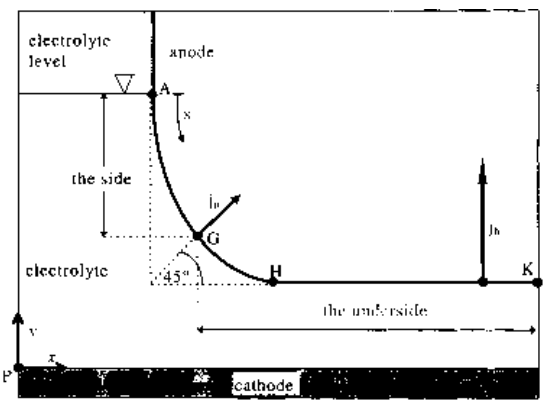

Fig. 2. Schematic representation of a vertical cross section of a cell with prebaked anode. Border between side and underside of anode are defined in point G. Current on flat part of anode, j_b; current density on side of the anode, j_n. Point P represents the origin of x, y coordinates.

where AlF_4^- is one of the aluminium fluoride complexes which may act as reactant. The potentials at which these reactions occur, are not known. The standard potential of aluminium carbide formation is 0.12 V positive to that of aluminium [26], but since the carbide is soluble in the electrolyte [27] its activity may be less than unity.

2.3. *Influence of the position of the sideledge on the current distribution*

In Part I [9] the current distribution was calculated for one case with a typical ledge shape (see Fig. 1(b)). To explore the influence of the position of the frozen ledge on the current distribution in greater detail, four calculations were made with different positions of the ledge. The above mentioned assumptions were used with boundary conditions valid for SCD.

The shape of the sideledge is a very complicated matter and a discussion of the factors of importance is beyond the scope of the present paper. In principle the temperature at the electrolyte/ledge interface is equal to the liquidus temperature (t_{liq}) for primary crystallization of cryolite (Na_3AlF_6). The heat flux through the side (q) can be expressed by the equation $q = h(t_{bulk} - t_{liq})$, where h is the heat transfer coefficient and t_{bulk} is the electrolyte temperature. Due to the fact that h varies with the flow rate of the electrolyte and that the heat flux is not unidirectional, the ledge can take on a complex shape.

In this study the ledge shape given in Fig. 1(b) was selected on the basis of measurements by Thonstad, Kuang and Haarberg. Near the bath/metal interface the ledge is thinner due to higher heat transfer coefficients in that region. The suggested ledge shape is in a good agreement with that of Bruggeman and Danka [18]. The distance between the side ledge and the anode was varied between 10 and 40 cm. Similar ledge shapes and variation of the ledge to anode distance without significant changes in its shape (considering the part of the ledge in the electrolyte) were suggested by Ahmed *et al*. [20]. Arita *et al.* [17], Frazer *et al.* [22] and Schmidt- Hatting *et al.* [23] measured curvilinear ledge shapes in the bath in various cells.

2.4. *Influence of the shape of the ledge on the current distribution*

The effect of the angle γ between the sideledge and the horizontal, shown in Fig. 1(b), on the current distribution was studied. An additional set of 16 calculations was carried out for distances between the sideledge and the anode of 10, 20, 30 and 40 cm, respectively, changing the angle γ from 75° to 90°.

The influence of the shape of the sideledge on the electrode current densities was studied for different simulated shapes which were placed in the region D sketched in Fig. 1(b). To also evaluate the relation between the shape of the sideledge and the distance between the sideledge and the anode all the shapes were simulated for the distances x_1 of 15 and 30 cm, respectively. The value of $x_1 = 15$ cm was selected from the analysis of the results showing that nearly no variation of c.d.s at the side of the anode was observed for $x_1 = 20$ cm and 40 cm, while significant changes were found for $x_1 = 10$ cm compared to $x_1 = 20$ cm.

3. Results and discussion

3.1. *Difference between primary and secondary current distribution*

In Figs 3–7 the difference between PCD and SCD is shown for cases under consideration. Figure 3 shows the anodic current density against the vertical coordinate y for a 2.5 cm gap. At the upper part of the anode side the c.d.s for both the initial and steady state profiles are similar owing to the very small available space for the current lines. For the initial shape the current density (c.d.) at the top of the anode (21 cm) is 0.0003 A cm^{-2} for PCD and 0.066 A cm^{-2} for SCD. For the steady state shape the c.d. at the top is 0.002 A cm^{-2} for PCD and 0.082 A cm^{-2} for SCD, as shown in Table 1. When going towards the underside of the anode the c.d.s both for the initial and steady state shapes (for PCD) increase, and the curves differ significantly down to a vertical distance of 8 cm (counted from the metal surface) where they merge, ending at 4.5 cm (the underside of the anode) with the value of 0.75 A cm^{-2}. The c.d. behaves in the same way for SCD. The difference between PCD and SCD is pronounced only at the side of the anode. It should be noted that the calculated data for the initial shape for 2.5 and 10 cm gaps is strictly correct only when two new anodes are facing each other (due to the symmetry).

Compared to the 2.5 cm gap the 10 cm gap allows more space for the current lines, resulting in higher current densities at the anode side. For both distributions (PCD and SCD) and shapes the c.d.s at the side are higher than that in the previous case, as also shown by the c.d.s at the top of the anode (Table 1). The difference between the c.d.s for the initial and steady state shapes is also larger than that for the 2.5 cm gap. For the 30 cm gap these effects are even more pronounced. As can be seen from Fig. 4 the c.d.s at the side of the anode are higher than in the cases with 2.5 and 10 cm gaps. Below a vertical distance of 8 cm the difference between the PCD and SCD curves for both the initial and steady state shapes is less than in the previous cases.

In Fig. 5 the absolute difference in potentials between PCD and SCD is shown for the 30 cm gap at steady state. Potentials are used for the calculation of voltage drops in the electrolyte to obtain basic information of the electrical parameters of the cell. The maximum differences are at the upper part of the anode. For the initial shape near the upper half of the side of the anode the difference is 0.14 V. Down to-

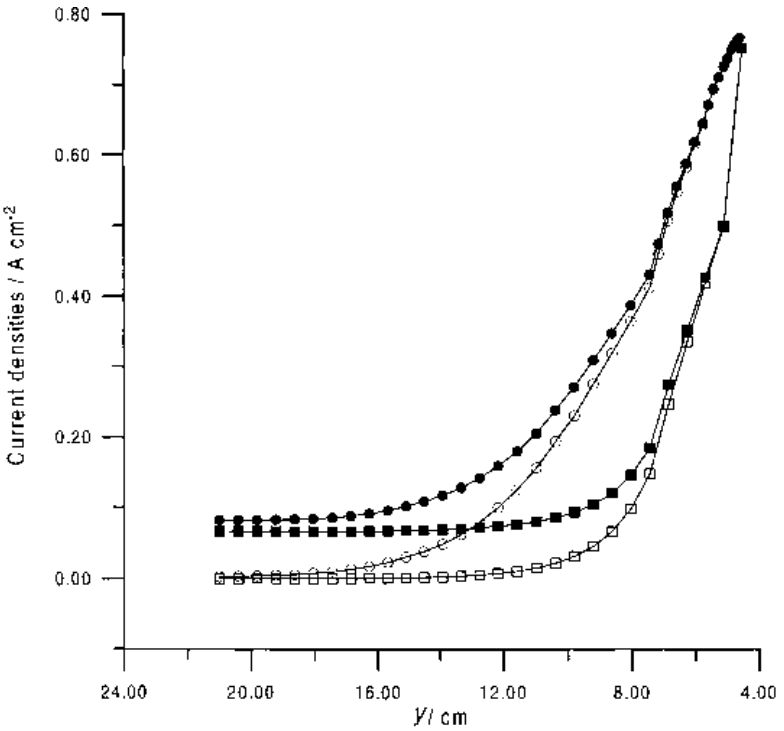

Fig. 3. Variation in anode current density in the y direction for 2.5 cm outside gap (5 cm distance between anodes). Anode shape is abbreviated to a.s. Key: (□—□—□) initial a.s. -PCD, (○—○—○) steady state a.s. -PCD, (■—■—■) initial a.s. -SCD, (●—●—●) steady state a.s. -SCD.

ward the bottom part of the anode it drops to 0.05 V. For the steady state (Fig. 5), the numbers are 0.08 and 0.001 V, respectively.

The cathodic c.d.s obtained for PCD and SCD differ little, owing to the low cathodic overvoltage and the use of a linear polarization curve (Equation 9) for SCD. In Fig. 6 the c.d.s along the cathode are shown for a 2.5 cm gap. The differences between the c.d.s for the initial and steady state shapes are large. In the calculated cross section of the cathode, the c.d. at point P, see Fig. 1(a), is 0.674 A cm^{-2} for PCD and 0.693 A cm^{-2} for the initial shape with SCD. The

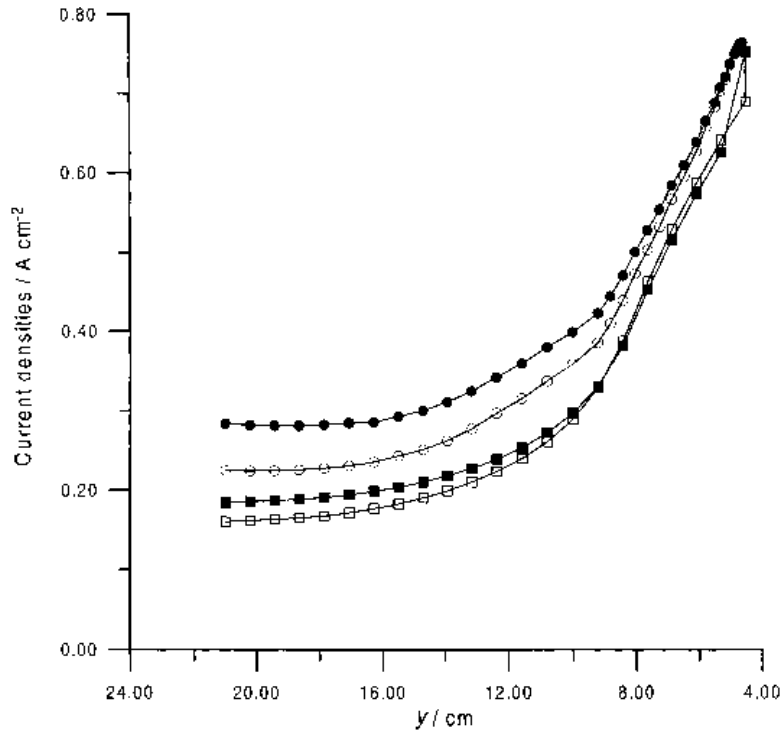

Fig. 4. Variation in anode current density as a function of y coordinate for 30 cm outside gap for initial and steady state shapes of the anode (a.s.). Key: (□—□—□) initial a.s. -PCD, (○—○—○) steady state a.s. -PCD, (■—■—■) initial a.s. -SCD, (●—●—●) steady state a.s. -SCD.

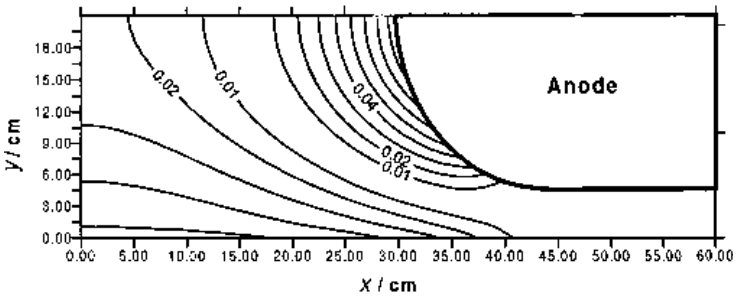

Fig. 5. Absolute difference in potentials between PCD and SCD for 30 cm outside gap and steady state anode shape. Potentials are in V, distances in cm.

steady state shape changes the geometry of the cross section, giving the corresponding values of $0.423\,\mathrm{A\,cm^{-2}}$ for PCD and 0.450 for SCD. When moving to the flat bottom part of the anode the c.d.s increase to the value of $0.75\,\mathrm{A\,cm^{-2}}$ at $x = 10$ cm for both PCD and SCD for the initial shape and at 20 cm for the steady state shape. The changes in the geometry of the calculated cross sections are not so pronounced for 10 and 30 cm gaps. The difference between the c.d.s for PCD and SCD is low, as seen in Fig. 7. In all cases the largest difference is located close to point P, see Fig. 1(a) (about 10%).

A qualitative description of the local current densities at the anode and similarly at the cathode can be expressed using the equation

$$j_{r,\mathrm{A}} = f_{\mathrm{A}}\left(Wa_{\mathrm{A}}, Wa_{\mathrm{C}}, x_r, y_r, z_r, \frac{\mathrm{L}_1}{\mathrm{L}}, \frac{\mathrm{L}_2}{\mathrm{L}}, \ldots, \frac{\mathrm{L}_n}{\mathrm{L}}\right) \quad (10)$$

where:

$$j_{r,\mathrm{A}} = \frac{j_{n,\mathrm{A}}(x,y)}{j_{\mathrm{b}}} \quad (11)$$

$$Wa_{\mathrm{A}} = \left(\frac{\mathrm{d}\eta_{\mathrm{A}}}{\mathrm{d}j}\right)_{j_{\mathrm{b}}}\left(\frac{1}{\rho_{\mathrm{E}}L}\right) \quad (12)$$

$$Wa_{\mathrm{C}} = \left(\frac{\mathrm{d}\eta_{\mathrm{C}}}{\mathrm{d}j}\right)_{j_{\mathrm{b}}}\left(\frac{1}{\rho_{\mathrm{E}}L}\right) \quad (13)$$

$$x_r = \frac{x}{L} \quad (14)$$

$$y_r = \frac{y}{L} \quad (15)$$

and $L_1/L, \ldots, L_n/L$ are dimensionless parameters of the system. Equations 12 and 13 are the Wagner numbers for the system, being equal to zero for PCD. The location of $j_{r,\mathrm{A}}$ at the anode surface is given by the coordinates x_r and y_r. In Equations 10–15 the characteristic dimension of the system under study is denoted as L. The characteristic length L can be chosen arbitrarily, for example, it may be the anode–cathode distance. In the present case we used L_1 as

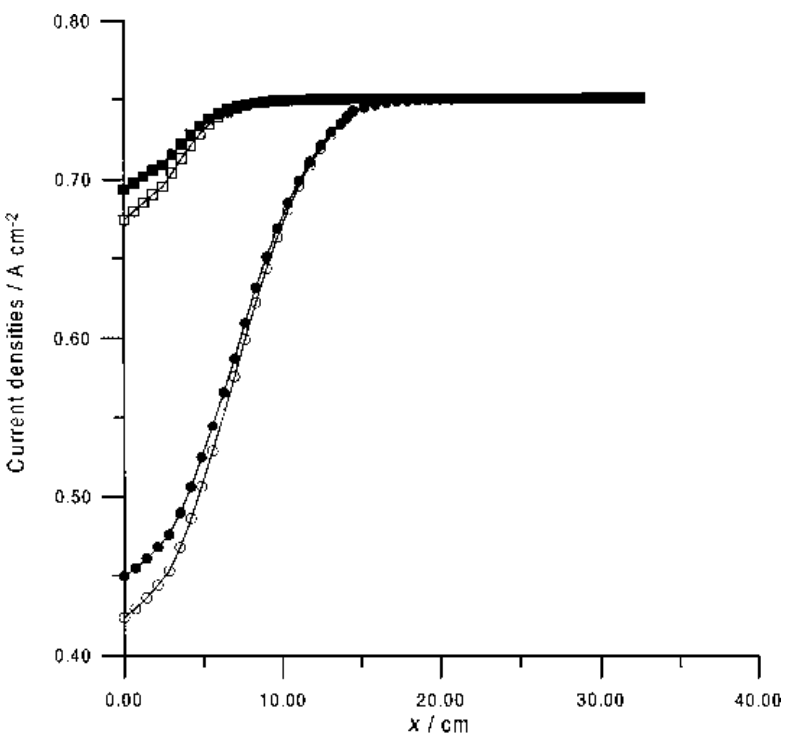

Fig. 6. Current density along cathode for 2.5 cm outside gap. Key: (□—□—□) initial a.s. -PCD, (○—○—○) steady state a.s. -PCD, (■—■—■) initial a.s. -SCD, (●—●—●) steady state a.s. -SCD.

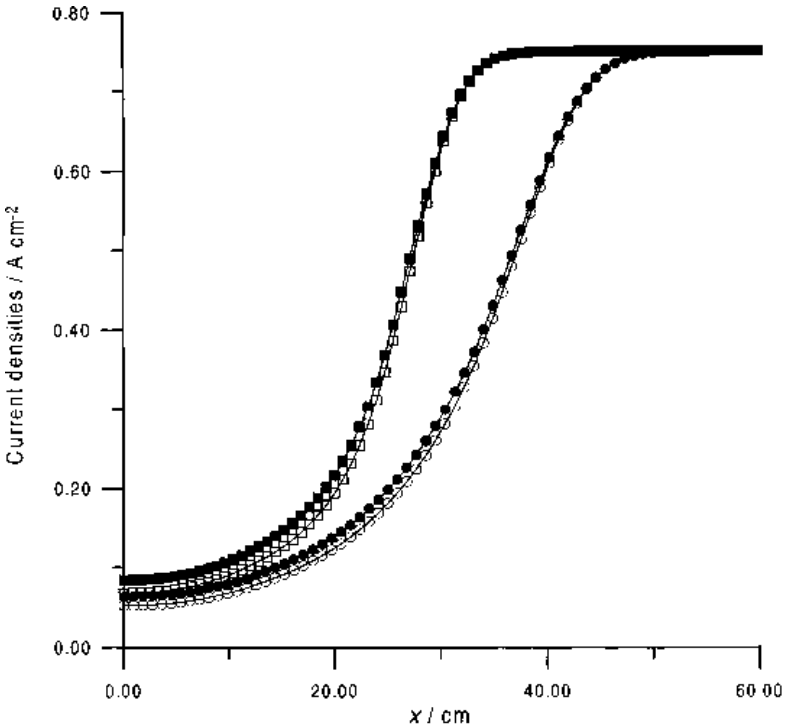

Fig. 7. Current density along cathode for 30 cm outside gap. Key: (□—□—□) initial a.s. -PCD, (○—○—○) steady state a.s. -PCD, (■—■—■) initial a.s. -SCD, (●—●—●) steady state a.s. -SCD.

the longest distance from the initial side of the anode to the side of the ledge, see Fig. 1(a).

A comparison of systems with different L_1 can be made for cases with constant $L_1, L_2, \ldots, L_n$ in such a way that all constant values be removed from Equation (10), and in the Wagner numbers the length L_1 will be used instead of L. Then follows from Equation 10:

$$\frac{j_n(T, L_1)}{j_b} = f'_A(Wa_A, Wa_C) \tag{16}$$

for SCD and

$$\frac{j_n(T, L_1)}{j_b} = f'_A(0, 0) \tag{17}$$

for PCD.
Elimination of j_b from Equations 16 and 17 gives the following:

$$\frac{j_n(T, L_1,\ \text{secondary})}{j_n(T, L_1,\ \text{primary})} = g(Wa_A, Wa_C) \tag{18}$$

Table 1. Current densities (in A cm^{-2}) at the top of the anode (point A in Fig. 2) for the three calculated cross sections (2.5, 10 and 30 cm, respectively) for PCD and SCD

Gap / cm	*Current density at top of anode* / A cm^{-2}			
	Initial shape of anode		*Steady state shape of anode*	
	PCD	SCD	PCD	SCD
2.5	0.0003	0.066	0.002	0.082
10	0.056	0.113	0.127	0.193
30	0.160	0.184	0.225	0.282

Equation 18 allows a simple comparison of c.d.s in point T on the anode for different cases, as shown in Table 2. The results in Table 2 agree well with the theoretical prediction of an increase of the j_{sec}/j_{prim} ratio with increasing Wagner number [8]. If we compare the same geometry for the cases of 30, 10 and 2.5 cm outside gap, respectively, it follows that the Wagner number increases when decreasing the characteristic length L_1.

3.2. *Current going through a sidewall partially covered by ledge*

In Fig. 8 the c.d.s along the cathode boundary are shown for SCD, 30 cm outside gap and a steady state anode shape (Fig. 1(a)). The length of the cathode boundary was taken as abscissa because it was also assumed that the sidewall acts as cathode. In the cases explained above, the cathode boundary length in Fig. 8 was calculated as the length of the boundary along the sidewall (the length in the y direction from M to P in Fig. 1(a)) continuing along the horizontal cathode (in the x direction). Figure 8 shows that there

Table 2. Dependence on Wagner's number on the ratio between the c.d. for SCD and for PCD

Gap/ cm	L_1 / cm	Wa'_A	$j(T,L_1,\text{sec})$	$j(T,L_1,\text{prim})$	$\frac{j(T,L_1,sec)}{j(T,L_1,prim)}$
2.5	2.5	0.124	0.066	0.0003	220
10	10	0.0311	0.113	0.05697	1.995
30	30	0.010	0.184	0.16002	1.157

Point T is identical with point A in Fig. 2.

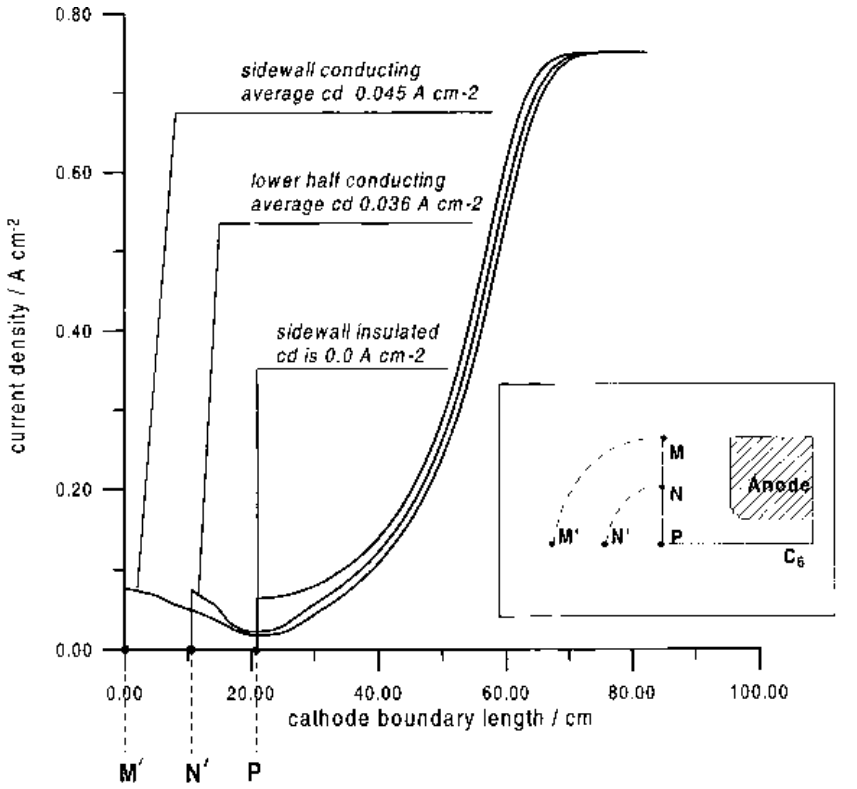

Fig. 8. Cathodic current densities along the cathode and the sidewall (calculated for geometry shown in Fig. 1(a), SCD, $x_1 = 30$ cm). Origin of distance measured for cathode is in point M. Distance from M to P represents the vertical part of the cathode. Aluminium cathode is located between points P (21.5 cm) and C_6 for all cases: (i) vertical part M–P of sidewall is conducting, (ii) vertical part N–P of sidewall is conducting, (iii) sidewall is insulated.

is a minimum at point P in all cases. The current through the sidewall is in average 0.045 A cm^{-2} or 0.95 A per cm sidelining (0.045 A cm$^{-2}\times$ height of the sidewall (21 cm, see Fig. 1(a))) when the whole sidewall is conducting, and 0.036 A cm^{-2} or 0.38 A per cm sidelining (0.036 A cm$^{-2}\times$ height of the half of the sidewall (10.5 cm, see Fig. 1(a))) when only the lower half of it is conducting. In all three cases the influence of the sidewall current on the anode current densities was less than 7% (due to the long distance of 30 cm). For a 75 cm wide anode facing a bare sidewall, the current passing through the sidewall will be 72 A, or 0.96% of a total load 7500 A. Calculated for all the anodes in a 150 kA cell, see Fig. 1(a) in [9], and neglecting the corner effects, the value is 1.6%.

If we assume that all the current going to the sidewall is used for aluminium carbide production (Equation 6) and subsequent dissolution in the electrolyte [27] the rate of wear of the sidewall (density 1.55 g cm^{-3}) will be 0.08 cm per day of exposure. Taylor *et al.* [28] measured a wear rate of 0.13 cm per day in industrial cells on an exposed sidewall. Gudbransen *et al.* [29] studied the wear of a graphite cathode in a laboratory cell with mechanical stirring and found that carbide formation and dissolution (named cathodic dissolution of carbon) occurred at 80% current yield up to a limiting c.d. of 0.10–0.11 A cm^{-2}. This value is higher than the sidewall currents calculated above, indicating that carbide formation and dissolution are the dominating reactions at an exposed sidewall.

3.3. *Influence of the distance to the side ledge on current distribution*

Four calculations were carried out with the shape of the ledge as sketched in Fig. 1(b) and the distances $x_1 = 10, 20, 30$ and 40 cm, respectively, under the conditions explained above. The distance x_1 between the ledge and the anode side influences the slope of the cathodic current density curves presented in Fig. 9. As the ledge profile moves towards the anode, the slope to the curve becomes steeper. Also the cathodic c.d.s in the outside channel become larger when the width of the outside channel between the ledge and anode decreases.

In Fig. 10 the influence of the distance x_1 between the ledge and the anode side on the anodic densities is shown. The length of the anode boundary (depicted as 's' in Fig. 2) was taken as the abscissa, representing the physical length of the boundary going from the uppermost anode boundary point (point A in Fig. 2) to the underside of the anode (5 cm to the right of point H in Fig. 2). Beyond that point the c.d. has a constant value of 0.75 A cm^{-2} in all cases. As can be seen from Fig. 10 the width of the outside channel (sideledge–anode gap) affects the c.d.s on the anode side only at the upper part. At the lower half of the anode side the differences between the c.d.s is less than 10%. The resistance of a narrow outside channel is higher than the resistance of the wide outside channel. This result in low c.d.s at the upper part of the side of the anode for a narrow outside channel.

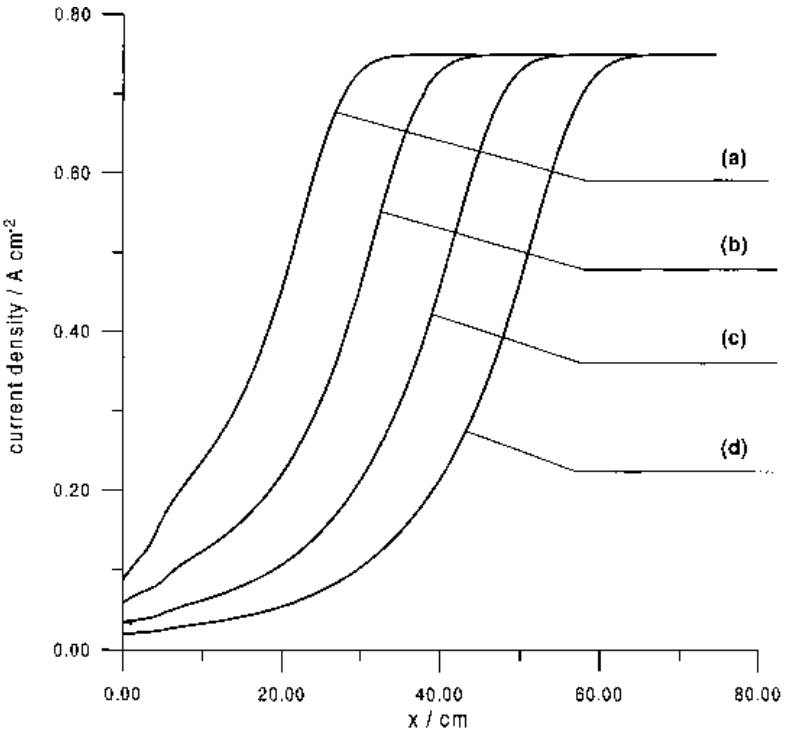

Fig. 9. Cathodic current densities along the cathode for cell with a ledge shape described in [9], Fig. 1(b). (Calculated for steady state anode profile shown in Fig. 1(b), steady state anode shape calculated for $L_1 = 30$ cm, with SCD.) Outside gaps, x_1: (a) 10, (b) 20, (c) 30 and (d) 40 cm, respectively. Origin of x coordinate is placed in the point P, see Fig. 1(a).

3.4. *Influence of the slope of the sideledge of the current distribution*

A set of calculations of current distribution was carried out varying the angle γ, shown in Fig 1(b). Variation of the angle γ between 75° and 90° for the distances x_1 of 10, 20, 30 and 40 cm, respectively, produced very small changes in the anodic c.d.s. As can be seen from Table 3 and 4 for 10 and 40 cm gaps, variations in the angle γ affect both the anodic and cathodic c.d.s to a minor degree. The narrower the outside channel (the sidewall–anode gap), the more

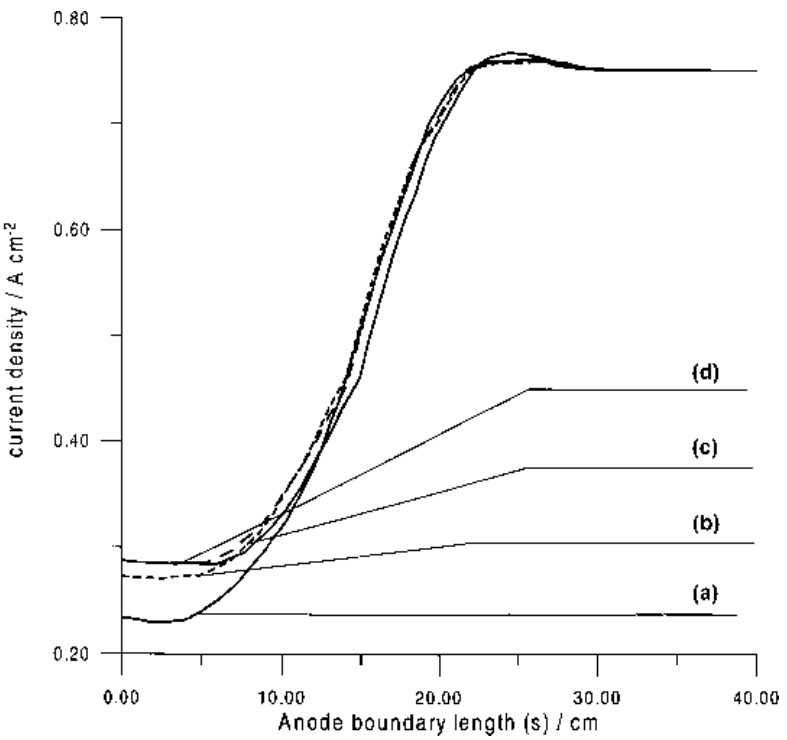

Fig. 10. Anodic current densities along anode for cell with ledge shape described in [9], Fig. 1(b). (Calculated for the geometry shown in Fig. 1(b), steady state anode shape calculated for $L_1 = 30$ cm, SCD.) Outside gaps, x_1: (a) 10, (b) 20, (c) 30 and (d) 40 cm respectively. Coordinate 's' is measured along anode boundary. Origin of 's' is located in A, see Fig. 2.

Table 3. Anodic current densities at points A_1–A_6 obtained for different angles γ between the sideledge and the horizontal (shown in Fig 1(b)) for the distances x_1 of 10 and 40 cm

x_1 / cm	γ / deg	A_1 / cm $^*x = 14.57$ $y = 21.00$	A_2 / cm $^*x = 16.16$ $y = 17.00$	A_3 / cm $^*x = 17.90$ $y = 13.10$	A_4 / cm $^*x = 20.42$ $y = 8.82$	A_5 / cm $^*x = 26.00$ $y = 5.00$	A_6 / cm $^*x = 44.50$ $y = 4.50$
10	75	0.203	0.205	0.265	0.413	0.733	0.750
	80	0.213	0.210	0.267	0.413	0.733	0.750
	85	0.220	0.214	0.268	0.413	0.733	0.750
	90	0.226	0.217	0.270	0.414	0.733	0.750
40	75	0.286	0.270	0.310	0.437	0.735	0.750
	80	0.286	0.270	0.310	0.437	0.735	0.750
	85	0.286	0.270	0.310	0.437	0.735	0.750
	90	0.286	0.270	0.310	0.437	0.735	0.750

* For $x_1 = 40$ cm the coordinates x of the points A_1–A_6 have to be calculated as $x + 30$ cm.

Table 4. Cathodic current densities at points C_1–C_6 obtained for different angles γ between the sideledge and the horizontal (shown in Fig. 1(b)) for the distances x_1 of 10 and 40 cm

x / cm	γ / deg	C_1 / cm $x = x_e - 40$ $y = 0.00$	C_2 / cm $x = x_e - 35$ $y = 0.00$	C_3 / cm $x = x_e - 30$ $y = 0.00$	C_4 / cm $x = x_e - 20$ $y = 0.00$	C_5 / cm $x = x_e - 10$ $y = 0.00$	C_6 / cm $x = x_e - 0.0$ $y = 0.00$
10	75	0.158	0.217	0.306	0.622	0.750	0.750
	80	0.163	0.220	0.307	0.622	0.750	0.750
	85	0.168	0.222	0.307	0.622	0.750	0.750
	90	0.173	0.223	0.307	0.622	0.750	0.750
40	75	0.137	0.202	0.286	0.603	0.750	0.750
	80	0.136	0.202	0.286	0.603	0.750	0.750
	85	0.136	0.202	0.286	0.603	0.750	0.750
	90	0.128	0.202	0.286	0.603	0.750	0.750

Coordinate x_e belongs to the point C_6 as seen in Fig. 1(b). For $x_1 = 10$ cm, $x_e = 44.57$ cm and for $x_1 = 40$ cm, $x_e = 84.57$ cm.

pronounced are the differences in c.d. Table 3 gives the anodic c.d.s at the points A_1–A_6 shown in Fig. 1(b) for different angles γ. When varying the angle the c.d.s change slightly at the side of the anode but not at the underside. At the top (point A_1), the c.d.s for the angle γ of 75° and 90° differ by 10% for the 10 cm outside gap and by only 0.7% for the 40 cm gap.

As shown in Table 4 also the cathodic c.d.s vary with the angle γ, the maximum difference being at point C_1; e.g. for 10 cm gap the difference in c.d.s for the angles of 75° and 90° is 8.9% and for 40 cm gap 6.2%. It can be concluded that variations of the angle γ did not produce significant changes in the c.d.s. and the distance between the sideledge and the anode (x_1) has a greater influence.

Several calculations for different shapes of the sideledge positioned at $x_1 = 15$ and 30 cm from the anode side [24] showed that when there is at least 15 cm gap between the anode and the sideledge, any variation in the ledge boundary (sideledge shape) produces negligible differences in the c.d.s at the anode. Very different ledge shapes were placed in the region D, in Fig. 1(b), and for all cases the difference in anodic c.d.s was of the order of 0.1%. The given values of anodic c.d.s are valid for any possible ledge shape located in zone D for $x_1 > 15$ cm.

References

[1] K. J. Fraser, D. Billinghurst, K. L. Chen and J. T. Keniry, 'Light Metals 1989' (edited by P. G. Campbell), TMS, Warrendale, PA (1989), 219–26.

[2] W. W. Hyland, 'Light Metals 1984' (edited by J. P. Mc. Geer), TMS, Warrendale, PA (1984), pp. 711-20.

[3] P. A. Solli, T. Haarberg, T. Eggen, E. Skybakmoen and A. Sterten, 'Light Metals 1994' (edited by U. Mannweiler), TMS, Warrendale PA (1994), pp. 195–203.

[4] J. Zoric, I. Rousar, J. Thonstad and Z. Kuang, *J. Appl. Electrochem.* **26** (1996) 795–802.

[5] M. Matlosz, C. Creton, C. Clerc and D. Landolt, *J. Electrochem. Soc.* **134** (1987) 3015.

[6] M. Sorlie and H. Oye, 'Cathodes in Aluminium Electrolysis', Aluminium- Verlag, Dusseldorf (1989).

[7] J. Thonstad and Z. Kuang, *J. Appl. Electrochem.* **26** (1996) 481–86.

[8] D. P. Ziegler, 'Light Metals 1991' (edited by E. Rooy), TMS, Warrendale, PA (1991), pp. 363–74.

[9] J. Zoric, I. Rousar and J. Thonstad, *J. Appl. Electrochem.*, submitted.

[10] A. Johnsen, S. T. Kvamme, O. Lindheim and A. Slattavik, Proceedings of the VIII Al Symposium, Slovak–Norwegian Conference on Aluminium Smelting Technology (1995), pp. 143–48.

[11] M. V. Swain and E. R. Seguit, *J. Aust. Ceram. Soc.* **20** (1984) 9–12.

[12] A. T. Taberaux and A. Fickel, 'Light Metals 1994' (edited by U. Mannweiler), TMS, Warrendale, PA (1994), pp. 483–91.

[13] B. J. Welch and A. E. May, 8th Internationale Leichtmetalltagung, Leoben- Wien (1987), pp. 120–25.

[14] W. E. Haupin, *J. Met.* **23** (7) (1971) 41–4.

[15] J. J. J. Chen, C. C. Wei, S. Thomson, B. J. Welch and M. P. Taylor, 'Light Metals 1994' (edited by U. Mannweiler), TMS, Warrendale, PA (1994), pp. 285–93.

[16] B. Sulmont and G. Hudault, 'Light Metals 1978' (edited by J. Miller), TMS, Warrendale, PA (1978), 73–86.
[17] Y. Arita, N. Urata, H and Ikeuchi, *ibid.* ,, pp. 59–71.
[18] J. N. Bruggeman and D. J Danka, 'Light Metals 1990' (edited by M. Bickert), TMS, Warrendale, PA (1990), pp. 203–9.
[19] H. Pfundt, D. Vogelsang and U. Gerling, 'Light Metals 1989', TMS, Warrendale, PA (1989), pp. 371–77.
[20] H. A. Ahmed, S. M. El- Raghy, F. A. Elrefaie, S. Read and Z. Bassuny, 'Light Metals 1994' (edited by U. Mannweiler, TMS, Warrendale, PA (1994), pp. 333–38.
[21] A. Valles, V. Lenis and M. Rao, 'Light Metals 1995' (edited by H.O. Bohner), RMS, Warrendale, PA (1995), pp. 309–13.
[22] K. J. Frazer, M. P. Taylor and A. M. Jenkin, 'Light Metals 1990'. (edited by M. Bickert), TMS, Warrendale, PA (1990), pp. 221–26.
[23] W. Schmidt-Hatting, J. M. Blanc, J. C. Bessard and R. V. Kaenel, 'Light Metals, 1985', (edited by H.O. Bohner), TMS, Warrendale, PA (1985), pp. 609–24.
[24] J. Zoric, PhD thesis, University of Chemical Technology, Prague (1996).
[25] I. Rousar, K. Micka and A. Kimla 'Electrochemical Engineering', Elsevier, Amsterdam Academia, Praha (1986).
[26] JANAF Thermochemical Tables, US Department of Commerce, National Bureau of Standards, Washington, DC (1971, 1975).
[27] R. Odegard and A. Sterten, J. Thonstad, 'Light Metals 1987' (edited by R. D. Zabreznik), TMS, Warrendale, PA (1987), pp. 295–302.
[28] M. P. Taylor, B. J. Welch and J. T. Keniry, 'Light Metals 1983' (edited by E. M. Adkins), TMS, Warrendale, PA (1983), pp. 437–41.
[29] H. Gudbransen, A. Sterten and R. Odegard, 'Light Metals 1992' (edited by E.R. Cutshall), TMS, Warrendale, PA (1992), pp. 521–28.